Bifurcation analysis of electric field domains in semiconductor superlattices

M. Patra, G. Schwarz, F. Prengel and E. Schöll
Institut für Theoretische Physik, Technische Universität Berlin,
D-10623 Berlin – eMail: patra@lorenz.physik.tu-berlin.de

We theoretically investigate vertical high-field transport in semiconductor superlattices, which exhibit self-generated current oscillations and the formation of stable stationary electric field domains depending on the available carrier density. The corresponding bifurcations scenarios and phase diagrams are determined. We demonstrate how this behaviour is affected by growth-related imperfections like fluctuations of the doping density.

Introduction

We consider a semiconductor superlattice where electric field domains form in the growth direction under high-field conditions if the superlattice is sufficiently doped or optically excited [1, 2, 3, 4]. Previous studies have shown that the current-voltage characteristic consists of a sequence of branches (their number being roughly equal to the number of quantum wells), which arise from different locations of the domain boundary. These branches overlap in a certain range of the voltage, leading to multistability and different curves for sweep-up and sweep-down of the voltage [5]. Recently, time-dependent features like transient [6] and persistent oscillations have also been found both in simulations [7, 8] and experimentally [9].

We use a simple microscopic model presented in Refs. [10, 7] with an extension for disordered superlattice samples [11, 12, 13]. The superlattice consists of N GaAs quantum wells of width l separated by $N-1$ AlAs barriers of width b. The wells are n-doped with a doping concentration (per unit volume) $N_D^{(i)}$ in the ith well, the average doping density of all wells is N_D. In order to simulate realistic samples we assume that the doping density may differ at random from well to well. We model those frozen-in doping fluctuations by $N_D^{(i)} = N_D(1+\alpha e_i)$ where $N_D^{(i)}$ is the doping density in the ith quantum well. The amount of doping fluctuations is determined by the parameter α. The sequence $\{e_i\}$ consists of N random values from the interval $[-1, 1]$, which are taken to be fixed when α is changed.

We use the electron concentrations in the kth subband of the ith well, $n_k^{(i)}$ as the dynamic variables of our system. For simplicity we consider only the two lowest subbands, $k = 1, 2$. The rate of change of the carrier densities $n_k^{(i)}$ is given by

$$\dot{n}_1^{(i)} = n_2^{(i)}/\tau_{21} + R_1^{(i)} n_1^{(i-1)} - R_1^{(i+1)} n_1^{(i)} - n_1^{(i)}(X_r^{(i+1)} + X_l^{(i)}) + n_2^{(i+1)} Y_l^{(i+1)} + n_2^{(i-1)} Y_r^{(i)} \quad (1)$$

$$\dot{n}_2^{(i)} = -n_2^{(i)}/\tau_{21} + R_2^{(i)} n_2^{(i-1)} - R_2^{(i+1)} n_2^{(i)} - n_2^{(i)} (Y_l^{(i)} + Y_r^{(i+1)}) + n_1^{(i-1)} X_r^{(i)} + n_1^{(i+1)} X_l^{(i+1)} \quad (2)$$

where $\tau_{21} = 1$ ps is the intersubband relaxation time. $R_k^{(i)}$ is the rate of electrons crossing the ith barrier between equivalent subbands k of two neighbouring wells modelled by miniband conduction [10]. The tunnelling coefficients $X_r^{(i)}$, $X_l^{(i)}$, $Y_r^{(i)}$, and $Y_l^{(i)}$ for transitions between different subbands of neighbouring wells depend on the field $F^{(i)}$; the subscripts r and l denote resonant tunnelling to the right and left, respectively. X stands for transitions from the first to the second subband, and Y for the reverse process. They are calculated from perturbation theory [10]. $X_r^{(i)}$ and $Y_l^{(i)}$ exhibit a distinct maximum for large electric fields where the first and the second subband of adjacent wells are in resonance. The electric field $F^{(i)}$ can be calculated from Poisson's law $\epsilon(F^{(i+1)} - F^{(i)}) = e(n_1^{(i)} + n_2^{(i)} - lN_D^{(i)})$, where ϵ is the permittivity of GaAs. The fields have to satisfy $\sum_{i=1}^{N+1} (l+b) F^{(i)} = U$, where U is the voltage applied to the sample. The sample contacts are treated as two additional "virtual" wells denoted by $i = 0$ and i=$N+1$ for which the boundary conditions $n_1^{(i)} = 2N_D$ and $n_2^{(i)} = 0$ are assumed treating the contacts as a carrier reservoir [14]. The increased density of charge carriers is to model ohmic contacts which are created by heavily doping the boundary layers.

Simulations

For uniform or nearly uniform electric fields the current-voltage characteristic following from (1), (2) exhibits a two-peak-structure with a sharp maximum due to resonant tunnelling as shown in the inset of Fig. 3. At higher doping, spatio-temporal instabilities lead to self-oscillations of the current associated with the build-up of space-charges [7, 15]. At the highest doping densities, the number of available carriers is sufficient to provide the space charge necessary to form a stable boundary between a low-field and a high-field domain. Stationary domains are then found. This behaviour is summarized in Fig. 1 for a "perfect" superlattice. Limit cycle oscillations are generated by a supercritical Hopf bifurcation as is shown in Fig. 2. The inset depicts the evolution of the field distribution during limit cycle oscillations.

In Fig. 3 the current-voltage characteristic is displayed at a higher mean doping density where stable stationary high-field domains form at the anode in the NDC regime (cf. inset). Along the full connected current-voltage characteristic stable and unstable parts alternate. They correspond to a continuous shift of the domain boundary across the superlattice from the anode ($i = N$) to the cathode ($i = 1$) with on average increasing bias. On the ith stable part (with rising voltage) the domain boundary is pinned at the $(N-i)^{th}$ well, while along the unstable parts (with falling voltage) the boundary is shifted to the next well. For neighbouring stable branches the domain boundary is thus displaced by one superlattice period.

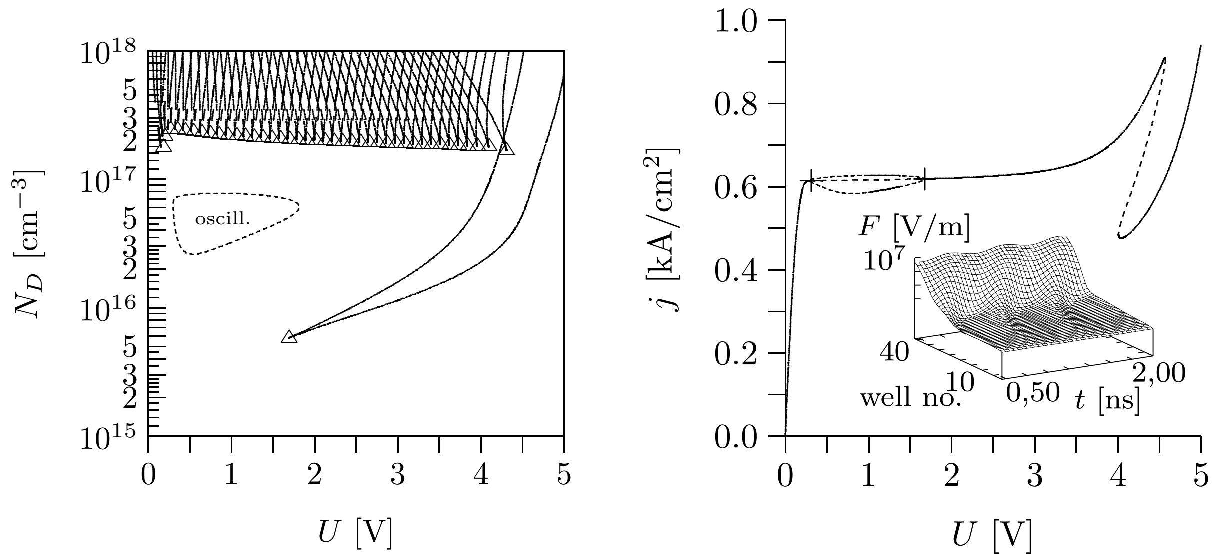

Figure 1 **(left)**: Phase diagram as a function of doping density N_D and bias voltage U for a "perfect" superlattice of $N = 40$ periods of GaAs/AlAs layers with $l = 90\,\text{Å}, b = 15\,\text{Å}$. Both the locations of supercritical Hopf bifurcations (dashed) and saddle-node bifurcations (full) are shown. The saddle-node bifurcations originate from cusp points (marked △) and indicate the existence of field domains.

Figure 2 **(right)**: Bifurcation scenario for fixed $N_D = 7 \cdot 10^{16}$ cm^{-3} (full lines: stable steady states, dashed lines: unstable steady states, dotted lines: limit cycle oscillations). The inset shows the evolution of the field distribution $F(x,t)$ during current self-oscillations.

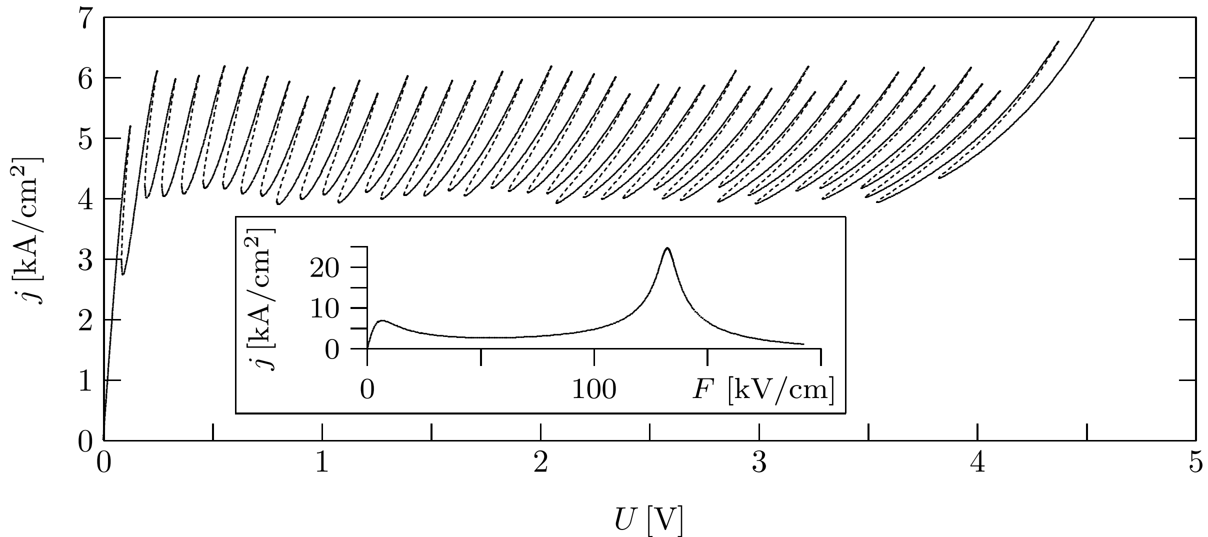

Figure 3: Current density j vs. voltage U and doping fluctuations of $\alpha = 4\,\%$ ($N_D = 7.9 \cdot 10^{17}$ cm^{-3}). Both stable (full) and unstable (dashed) domain states are shown. The inset depicts the current-voltage characteristic for uniform fields.

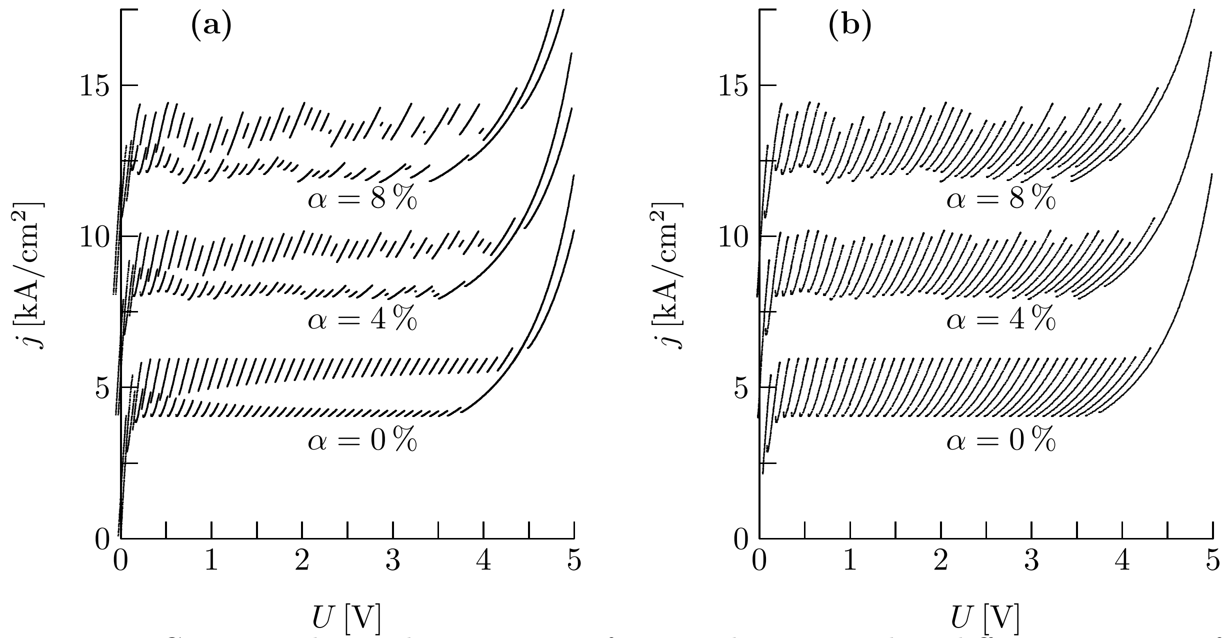

Figure 4: Current-voltage characteristics for superlattices with a different amount of doping fluctuations, **(a)** characteristics for voltage sweep-ups and sweep-downs, **(b)** stable parts of the full connected current-voltage characteristics ($N_D = 7.9 \cdot 10^{17}$ cm^{-3}; the vertical scale is shifted for each curve)

In the presence of doping fluctuations, the values of the voltage U and the current j, at which the stable branches become unstable, are varying for the individual branches. As the effects for the lower and the upper points are different, the length of the branches as well as their position is varying irregularly. However, there exists a direct correlation between the doping density $N_D^{(i)}$ in the ith quantum well and the height of the corresponding branch of the current-voltage characteristic for which the domain boundary is pinned in that well. Therefore, the current-voltage characteristic gives insight not only into the overall amount of fluctuations α but also into the doping densities of each individual quantum well.

In Fig. 4, the current-voltage characteristics are compared for different values of α. Upon voltage sweep-ups or sweep-downs the lengths of the parts of each stable branch, which can be reached in the simulation, are varying heavily (Fig. 4(a)). For high values of α some branches are missed out altogether, as a result of their reduced length. In Fig. 4(b) the corresponding full connected current-voltage characteristics are presented. Even for superlattices with high doping fluctuations the structure of the current-voltage characteristic does not change, only the lengths of the individual branches differ slightly. As during a voltage sweep-up or sweep-down only a small part of the whole stable branch is reached, these small changes in the lengths and positions of the individual branches are enlarged when compared to the full connected current-voltage characteristic.

Oscillations are also strongly affected by doping fluctions. However, this does not apply to their form or frequencies, but rather to the values of the parameters

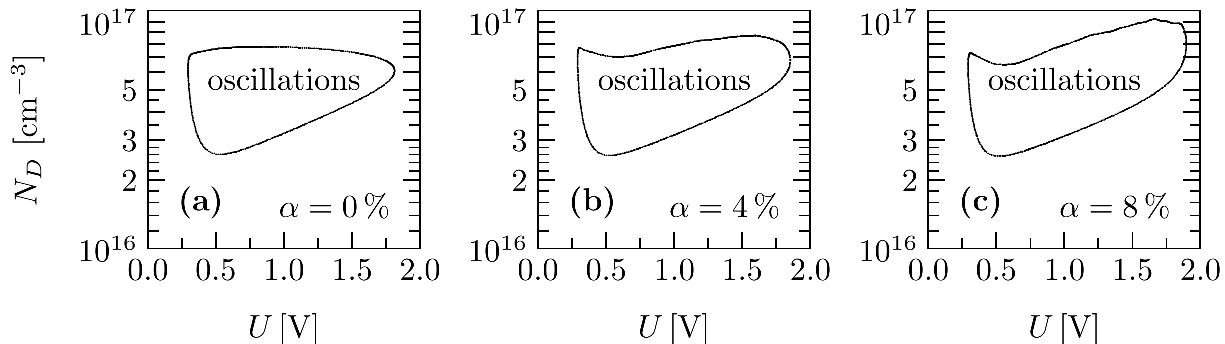

Figure 5: Phase diagram of spatio-temporal instabilities as a function of doping density N_D and bias voltage U for a superlattice of $N = 40$ periods of GaAs/AlAs layers with $l = 90\,\text{Å}, b = 15\,\text{Å}$. The full line marks the location of supercritical Hopf bifurcations. **(a)** Phase diagram for a perfect superlattice, **(b)**, **(c)** for a superlattice with $\alpha = 4\,\%$ respectively $\alpha = 8\,\%$, where $N_D^{(i)} = N_D\,(1 + \alpha e_i)$ with a random set of N values e_i from the interval [-1,1].

doping density N_D and voltage U, for which the system exhibits spatio-temporal instabilites. Phase diagrams for three different values of α are presented in Fig. 5. The shape of the area of the oscillatory regime in control parameter space does not only depend strongly on the overall amount of fluctuations α, but even more critically on the precise realisation of the individual fluctions $\{e_i\}$ in each quantum well.

In conclusion, we emphasize that important aspects of the dynamics of semiconductor superlattices, especially irregularities, express themselves in the current-voltage characteristic, which can also be determined experimentally. Therefore, by simple global macroscopic electric measurements, in combination with model calculations, microscopic structural features can thus be investigated.

We would like to thank H. T. Grahn, J. Kastrup, and A. Wacker for their cooperation. This work was supported by DFG in the framework of Sfb 296.

References

[1] L. Esaki and L. L. Chang, Phys. Rev. Lett. **33**, 495 (1974).

[2] K. K. Choi, B. F. Levine, R. J. Malik, J. Walker, and C. G. Bethea, Phys. Rev. B **35**, 4172 (1987).

[3] H. T. Grahn, R. J. Haug, W. Müller, and K. Ploog, Phys. Rev. Lett. **67**, 1618 (1991).

[4] Y. Zhang, X. Yang, W. Liu, P. Zhang, and D. Jiang, Appl. Phys. Lett. **65**, 1148 (1994).

[5] J. Kastrup, H. T. Grahn, K. Ploog, F. Prengel, A. Wacker, and E. Schöll, Appl. Phys. Lett. **65**, 1808 (1994).

[6] R. Merlin, S. H. Kwok, T. B. Norris, H. T. Grahn, K. Ploog, L. L. Bonilla, J. Galán, J. A. Cuesta, F. C. Martínez, and J. M. Molera, in *Proc. 22nd Int. Conf. Phys. Semicond., Vancouver 1994*, edited by D. J. Lockwood (World Scientific, Singapore, 1995), p. 1039.

[7] A. Wacker, F. Prengel, and E. Schöll, in *Proc. 22nd Int. Conf. Phys. Semicond., Vancouver 1994*, edited by D. J. Lockwood (World Scientific, Singapore, 1995), Vol. 2, p. 1075.

[8] L. L. Bonilla, J. Galán, J. A. Cuesta, F. C. Martínez, and J. M. Molera, Phys. Rev. B **50**, 8644 (1994).

[9] J. Kastrup, R. Klann, H. T. Grahn, K. Ploog, L. L. Bonilla, J. Galán, M. Kindelan, M. Moscoso, and R. Merlin, Phys. Rev. B **52**, 13761 (1995).

[10] F. Prengel, A. Wacker, and E. Schöll, Phys. Rev. B **50**, 1705 (1994).

[11] A. Wacker, G. Schwarz, F. Prengel, E. Schöll, J. Kastrup, and H. T. Grahn, Phys. Rev. B **52**, 13788 (1995).

[12] G. Schwarz, A. Wacker, F. Prengel, E. Schöll, J. Kastrup, H. T. Grahn, and K. Ploog, Semicond. Sci. Technol. (1996), in press.

[13] E. Schöll, G. Schwarz, M. Patra, F. Prengel, and A. Wacker, in *Proc. 9th Int. Conf. on Hot Carriers in Semiconductors, Chicago 1995*, edited by K. Hess, J. P. Leburton, and U. Ravaioli (Plenum Press, New York, 1996), in print.

[14] G. Schwarz and E. Schöll, phys. status solidi (b) **194**, 351 (1996).

[15] L. L. Bonilla, in *Nonlinear Dynamics and Pattern Formation in Semiconductors*, edited by F. J. Niedernostheide (Springer, Berlin, 1995), Chap. 1, pp. 1–20.